Photoluminescence Spectroscopy on Optically Pumped Semiconductor Disk Lasers

Frank Demaria and Alexander Hein

Photoluminescence spectra from optically pumped semiconductor disk lasers are presented. A detailled discussion of the results is given as well as a description of the measurement setup and procedure. Spectra which have been measured under different detection angles show specific features which are attributed either to the intrinsic photoluminescence of the gain region or to the distortion which arises from the optical resonances of the integral layer structure of the device. The influence of the extended resonator is investigated by applying the described technique to laser samples in configurations with and without external mirror.

1. Introduction

Photoluminescence (PL) spectra offer valuable insight to the basic physical characteristics and the principal behavior of optically pumped semiconductor disk lasers. PL arises from spontaneous emission processes which take place in the excited regions within the structure. The energy of the emitted photons is thereby determined by the difference of the energy states of the recombining carriers which is at least the band gap at their local position. Electrons and holes are generated by absorption of the incident pump radiation. Fundamental absorption processes can occur within the barriers or in the subbands of the quantum wells of the periodic gain structure [1]. From this point of view, the gain structure of an optically pumped disk laser is actually optically absorbing and amplifying at the same time. In the experiments described here, pumping is predominantly carried out within the barriers of a periodic gain structure designed for a laser emission wavelength of 920 nm. Barrier pumping is the most common way of optical pumping of semiconductor disk lasers as it is more straightforward than direct pumping of the quantum wells [2, 3]. Quantum well pumping on the other hand has the advantage of a smaller quantum defect energy given by the difference of the energy of the pump photons and the emitted laser photons [4]. Both approaches, however, require a thorough tuning of the optical resonances of the overall layer structure and the spectral absorption and amplification properties of the quantum wells to provide high efficiencies [5, 6]. Information on both is contained in the PL spectra. However, careful interpretation is necessary to designate the origin of observed spectral characteristics.

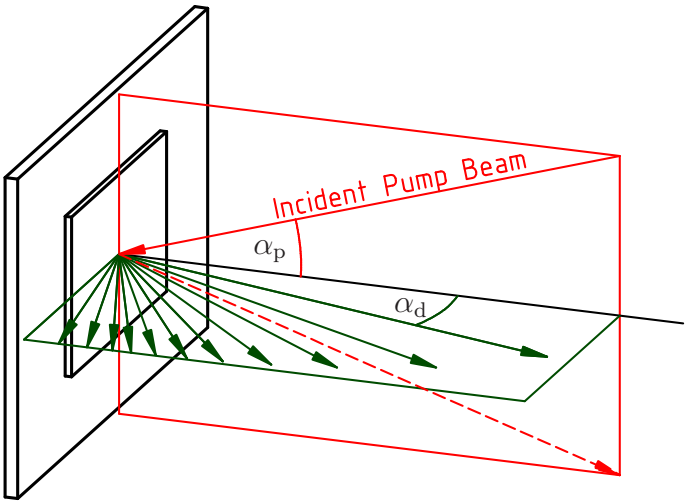

Fig. 1: Simplified arrangement of the experimental setup. Pump radiation is incident under the pump angle α_p in the vertical plane of incidence whereas the emitted PL spectrum is measured at the detection angle α_d in the horizontal plane. The thin semiconductor disk laser is mounted on a copper heat sink.

2. Experimental Setup and Design of the Disk Laser Chip

An outline of the basic geometrical arrangement of the experimental setup is given in Fig. 1. In the described experiments, optical pumping is realized at pump angles α_p between 20 ° and 30 °. At these values, the maximum absorptivity is provided for the pump wavelength, according to the layer design of the samples under investigation. The wavelength spectrum of the PL is measured at the detection angle α_d. To achieve best spatial separation between the reflected fraction of the pump beam and the emitted PL, the plane of detection is perpendicular to the plane of incidence of the pump beam. A fiber-coupled diode laser is used as a pump source. Its emission wavelength ranges between 799 and 804 nm, depending on the emitted pump power and the temperature of the cooling water. A simple arrangement of two lenses is used to focus the light from the 200 µm-core-diameter fiber to the laser sample which results in a mean pump spot diameter of approximately 0.4 mm. The pump beam possesses low spatial beam quality with a diffraction number of $M^2 \approx 55$ and therefore results in a full far-field angle of 8 ° for the given optical arrangement. This value has to be considered for the angle of convergence of the incident pump beam respectively for the divergence of its reflected fraction. It represents an inherent uncertainty of the pump angle.

Detection of the PL is realized by coupling to a fiber which is connected to an optical diffraction-grating spectrum analyzer. To do so, a lens with 14.5 mm focal length and an aperture of 8 mm is placed 130 mm away from the pumped area. That way, an angular resolution of less than 1.8 ° is established. The laser sample is soldered with indium on a gold plated copper heat sink whose temperature can be stabilized at arbitrary temperatures between −20 and +70 °C.

A detailled discussion of the layer design of sample #1 is given in [7] or our contribution to the last year's annual report [8]. Basically, sample #1 and #2 consist of a periodic gain structure [1] and a double-band Bragg reflector [9, 10]. The periodic gain structure of sample #1 is formed by a sequence of six 8 nm-thick $In_{0.08}Ga_{0.92}As$-GaAs quantum wells. The surrounding barriers of distinct quantum wells are separated by large bandgap $GaAs_{0.71}P_{0.29}$ strain compensation layers which also act as a carrier diffusion barrier.

Sample #2 contains a periodic gain structure with nine double quantum wells, consisting of 6 nm-thick $In_{0.08}Ga_{0.92}As$-GaAs quantum wells separated by a 6 nm barrier. The double-band Bragg reflector of both structures is designed to provide high reflectivity for the incident pump light and for the lasing wavelength within its two stop bands.

3. PL Spectra and Interpretation

3.1 Operation without external mirror

Typical photoluminescence spectra which have been taken from sample #1 are shown in Fig. 2. In this example, the influence of temperature and pump intensity variations can be observed. The spectra are detected at a constant angle of 20 °. Pumping is realized with a wavelength of 799 nm at a pump angle of 30 °. A distinct but low-intensity peak resulting from the pump light can be observed in the spectrum for low pump intensity and low temperature. It occurred also in the other spectra, however it is not shown there as the recorded data does not cover this wavelength.

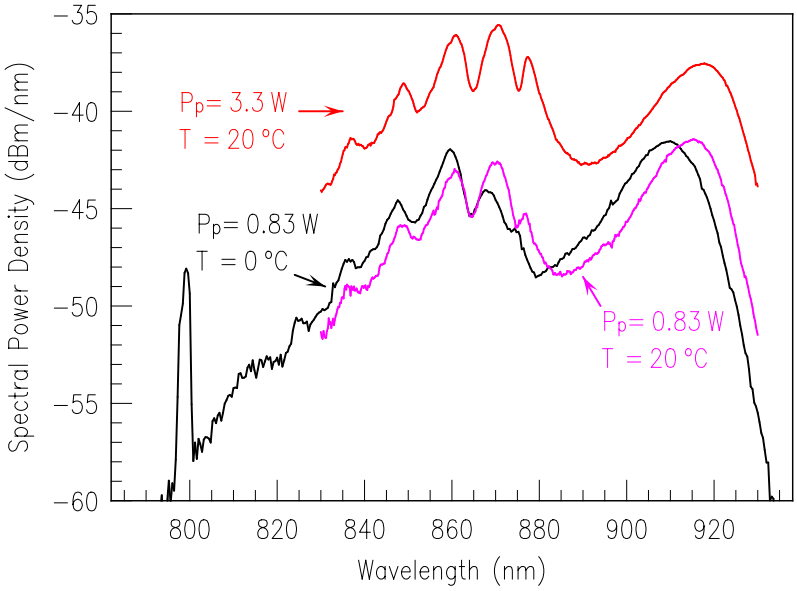

Fig. 2: PL spectra from laser sample #1 under operation without external resonator. All spectra are detected under an detection angle of $\lambda_d = 20\,°$ during operation with a pump angle of $\lambda_p = 30\,°$. The lower curves are measured at a temperature of 0 and 20 °C and refer to an optical pump power of 0.83 W which would be below threshold during laser operation with a standard external mirror. The upper curve with a heat sink temperature of 20 °C refers to an incident optical pump power of 3.3 W which would be significantly above threshold in operation with an external mirror.

Generally, all spectra can be divided into two distinct regions which represent photon energies below and above the band gap energy of the GaAs barriers. They are roughly separated by the valley around 880 nm. For the longer wavelength region, a broad smooth peak can be observed in all curves with a maximum between 910 and 920 nm. It represents the PL from the $In_{0.08}Ga_{0.92}As$ quantum wells. For the curves with weak pumping,

the maximum shifts from 909.5 nm at 0 °C to 915.5 nm at 20 °C. A wavelength shift of approximately 0.3 nm/K is usually attributed to the temperature dependent band-gap decrease.

The PL between 820 and 880 nm, has its origin in the GaAs barriers. Here, a pronounced modulation of the curves can be observed which leads to five local maxima. For a physical interpretation of the spectrum within this wavelength range it is necessary to distinguish between the broad substantial curve which represents the intrinsic PL from the gain structure and the short periodic modulation. The latter is connected to the inconstancy of reflectivity and phase which is introduced by the back sided Bragg reflector in this wavelength region. Fluctuations of reflectivity with the same origin can be observed in the measured reflectivity spectra shown in Fig. 3. Ultimately their maxima represent optical resonances within the whole structure.

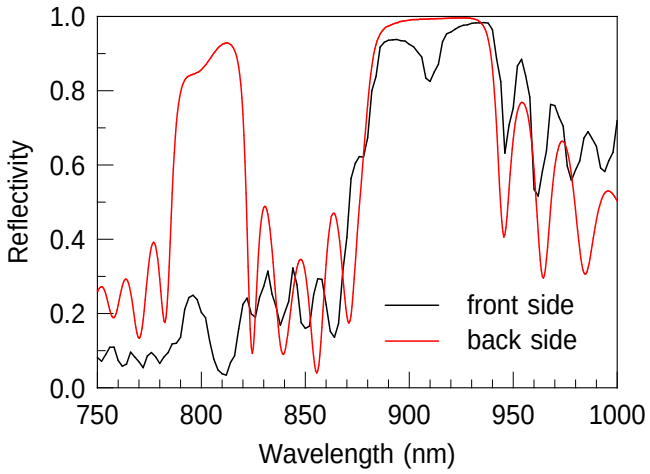

Fig. 3: Front and back side reflectivity spectra from sample #1 (same as in Fig. 2). Both are measured at a detection angle of 10 °. The back side spectrum was measured prior to metalization and mounting.

Whilst the intrinsic PL-curve shows a quite similar temperature offset above and below 880 nm, the temperature shift of the distinct resonances is significantly smaller. They arise basicly from the temperature dependent change of the optical layer thicknesses within the structure. Above 880 nm, no periodic modulation of the intrinsic curve takes place because it lies within the region of the broad stopband where a quite constant reflectivity and phase is introduced by the Bragg reflector.

The optical resonances can clearly be distinguished from the intrinsic PL curve when the angle of detection is varied. In this case, the resonance peaks move according to the cosine of the internal propagation angle. Their intensity, however, depends on the substantial PL at the particular wavelength which is independent from the detection angle. An example, which has been measured for sample #2 is given in Fig. 4. It shows an array of PL spectra for which the detection angle was varied from 0 to 90 °. The envelope of the curves roughly represents the intrinsic PL with its maximum around 873 nm for the barriers and at approximately 905 nm for the quantum wells. It is essential for this interpretation that the coupling into the fiber of the spectrometer was maximized at each detection angle with utmost care to guarantee a consistent coupling efficiency.

The observed resonance shift can be described fairly good with the direction cosine of the

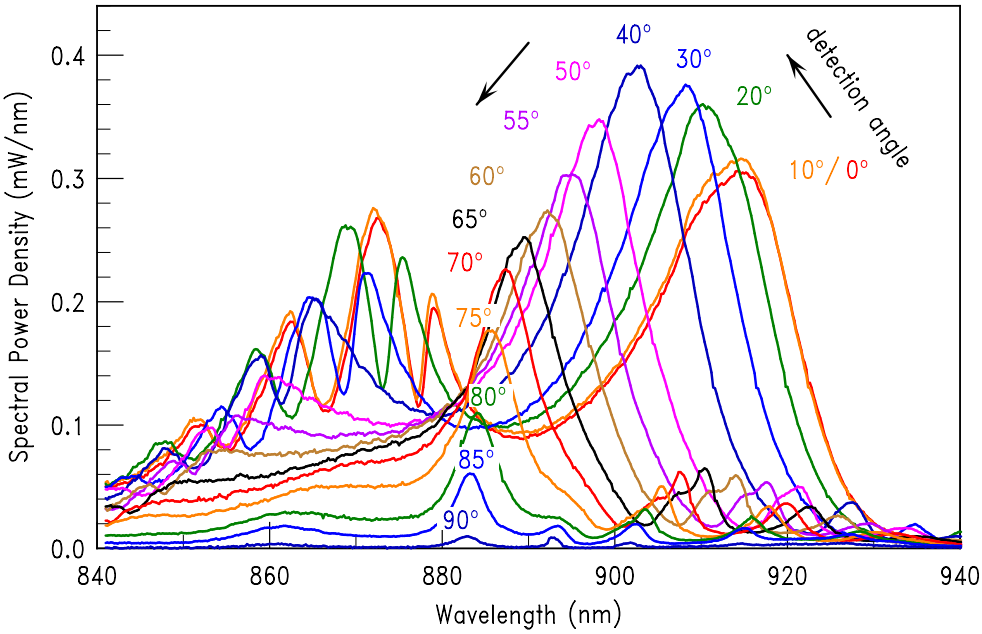

Fig. 4: PL spectra at different detection angles from sample #2. Pumping was realized with an optical pump power of 3.3 W at a heat sink temperature of 20 °C.

internally propagating optical wave

$$\lambda_{\mathrm{res}} = \lambda_0 \cos\beta, \tag{1}$$

wherein the internal propagation angle β can be deduced from the external propagation angle α_{d} by Snell's law, given by

$$\sin\beta = \frac{\sin\alpha_{\mathrm{d}}}{n_{\mathrm{eff}}}. \tag{2}$$

The influence of the layer structure is considered by the effective refractive index n_{eff}. Figure 5 shows a plot of the measured resonance wavelengths versus the detection angle, taken from Fig. 4, together with the fitted curve according to (1) and (2). From that, a

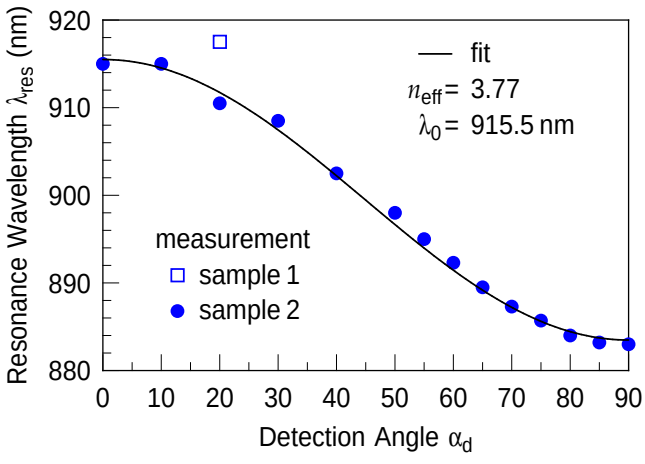

Fig. 5: The angular shift of the optical resonances from Fig. 4 (sample #2, dots) yields the effective refractive index n_{eff} and the resonance wavelength for perpendicular emission λ_0 as fit parameters from (1) and (2). The open square shows the resonance wavelength taken from Fig. 2 (sample #1) at the same temperature and pump intensity.

resonance wavelength for perpendicular emission of $\lambda_0 = 915.5\,\text{nm}$ and an effective refractive index $n_{\text{eff}} = 3.77$ can be deduced. The resonance wavelength actually determines the emission wavelength during laser operation. Obviously it is significantly shorter than the intended emission wavelength of 920 nm. The effective refractive index represents more or less an average value of the refractive index of the layer structure within the wavelength range under consideration. A quite important aspect is also at which wavelength and angle the maximum spectral PL intensity occurs. For sample #2 this is the case for 902.5 nm and 40 °, according to Fig. 4.

3.2 Laser operation with external mirror

Sample #1 reveals a comparatively good laser performance with a maximum optical output power above 4 W, which is shown in Fig. 6. The output characteristics has been recorded with external mirrors of 100 mm radius of curvature and reflectivities of 99 and 98 %. Emission wavelengths between 920 nm at threshold and 927 nm at maximum output power are observed. With sample #2 however, in the best case an optical output power of only 1 W was achieved in operation with an external mirror. Thereby, an emission wavelength between 913 nm at threshold and 916 nm at maximum optical output was observed.

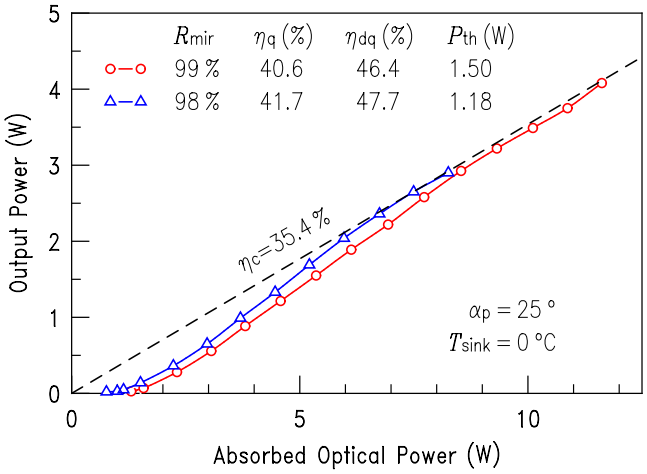

Fig. 6: Optical laser output characteristics of sample #1. A simple hemispherical resonator setup with external mirrors with 100 mm radius of curvature and reflectivities of 99 and 98 % was used. The larger threshold in operation with the mirror of higher reflectivity can be explained with a larger pump-spot diameter.

During the investigation of the PL spectra, an external mirror with 98 % and a radius of curvature of 150 mm was used. The output characteristic was not significantly changed by the different radius of the mirror.

PL spectra detected at 20 ° for various incident pump powers P_{p} are shown in Fig. 7. The heatsink temperature was stabilized at 0 °C which is the same value as for Fig. 6. All curves show a distinct peak from the pump laser which is slightly displaced from 800 nm to 801 nm with increasing pump power. Also the photoluminescence from both, the barriers and the quantum wells, can be distinguished clearly, much like in operation without external mirror from Fig. 2. Above threshold, in the curves with pump powers of 2.1 W and more, a distinct lasing peak arising from the stimulated emission of the quantum wells can be observed. It is important to note, that the laser light which establishes this peak

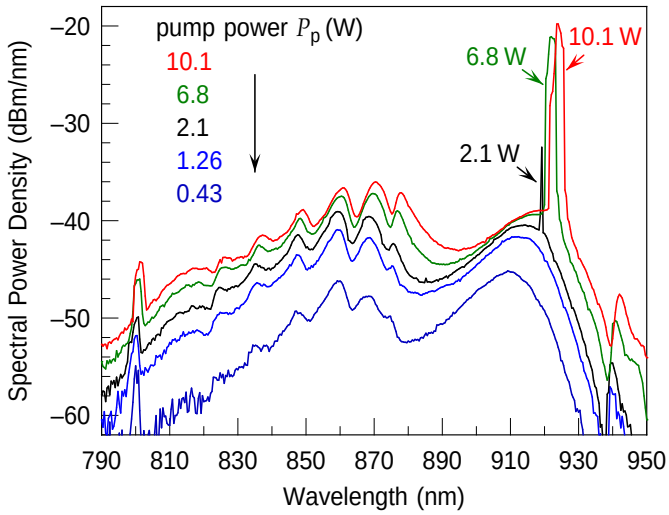

Fig. 7: PL spectra from sample #1 for various pump intensities below and above threshold in operation with an external mirror. All spectra are detected at an angle of 20 °. A mirror with a reflectivity of 98 % and a radius of curvature of 150 mm was used.

is not emitted through the external mirror. For the resonator length of approximately 100 mm, the external mirror with an aperture of 12.7 mm only covers detection angles up to 3.6 °. The difference becomes clear by comparing the 20 ° curves from Fig. 7 with the laser spectrum at an detection angle of 0 ° in Fig. 8 which was measured directly trough the outcoupling mirror. The measurement shown in Fig. 8 does not expose any spectral displacement of the laser peak for different detection angles. The reason is that much unlike the PL radiation in the rest of the spectra, the laser peaks which are detected at different angles are not related to a different direction of propagation within the laser's layer structure. The intensity of the laser peak, however, is decreasing with increasing detection angle. Both gives evidence that the detected laser light is predominantly redirected by diffraction and scattering.

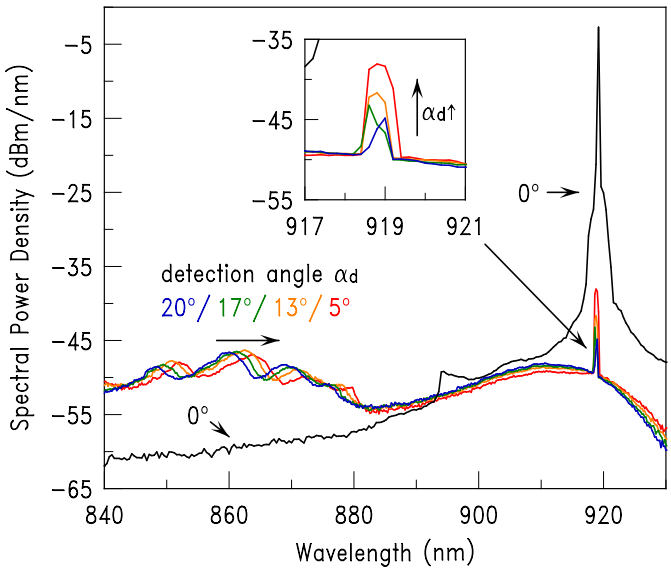

Fig. 8: PL spectra for various detection angles during laser operation with an optical pump power of 2.5 W for a heat sink temperature of 0 °C.

In Fig. 7, however, the wavelength of the laser emission is displaced for different pump intensities from 919 nm at 2.1 W to 924 nm at an incident pump power of 10.1 W. The local maxima of the resonances below 880 nm in the same measurement experience a smaller

displacement, much like in the measurement without an external resonator (Fig. 2). The displacement of the resonances is introduced mainly by the temperature dependent shift of the refractive index, whereas the shift of the lasing wavelength is related to the displacement of the spectral gain function. Remarkable is also that the intensity of the PL spectrum from the barriers (below 880 nm) increases much more than the PL intensity from the quantum wells (above 880 nm). With increasing pump intensity, the barriers become more and more populated with carriers whereas in the quantum wells, the carrier density is partially clamped. The observed increase of spontaneous emission in the barriers represents a considerable loss mechanism. A particular increase is indeed unavoidable because operation at high output powers requires a higher support of the quantum wells with carriers which is here a synonym for a higher diffusion current. This can, however, only arise from an enhanced gradient of the carrier concentration which in turn goes ahead with a higher concentration of carriers, especially in the barrier regions distant to the quantum wells.

Even though it is less pronounced, a continuous increase of the PL from the quantum wells indicates that also here, an entire clamping of the carrier density does not take place. This can particularly be explained by the reasonable assumption that the resonant gain structure is not homogeneously pumped both in the lateral and in the longitudinal direction. With increasing pump power, the non-uniform distribution of carriers over the quantum wells becomes even worse. This goes ahead with an enhanced PL, because in the regions with higher carrier density, spontaneous emission increases quadratically, due to the bimolecular recombination mechanism.

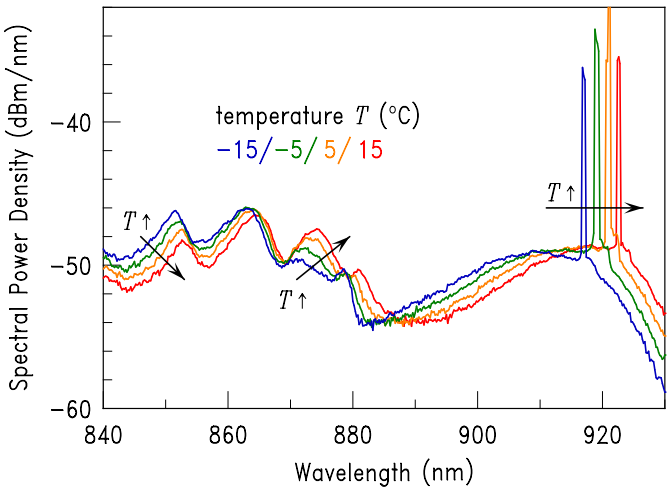

Fig. 9: PL spectra at a detection angle of $\alpha_d = 5°$ for various operation temperatures during laser operation. The optical pump power is 3.3 W for all curves.

For the sake of completeness, pure influence of a temperature change to the emitted PL and laser spectra is shown in Fig. 9. All spectra are measured at a detection angle of 5 ° with a constant optical pump power of 3.3 W. With increasing temperature, the laser peak shifts from 917.1 nm at -15 °C to 922.6 nm at 15 °C which corresponds to a spectral displacement of 0.183 nm/K. A quite similar shift can be observed for the substantial PL curves.

4. Conclusion and Outlook

We demonstrated a simple method to investigate spectral and angular resolved photoluminescence from optically pumped semiconductor disk lasers. The measurement technique can be applied for a pre-characterization of the samples prior to laser operation but also during operation of the devices in an extended resonator setup. The observed distortions of the spectra are correlated with longitudinal resonances within the layer structure of the sample. A decisive way to distinguish these resonances from the intrinsic photoluminescence is introduced by a variation of the detection angle. The resonance shift with the angle of measurement can be explained by the influence of the mean internal propagation angle. It can be calculated from Snell's law by the assumption of an effective refractive index for the layer structure. Its exact value can be evaluated from the measurement as a fit parameter.

Although measurements from two different samples have been presented, out major concern is rather to outline the principle of the measurement and to suggest an interpretation of the results, than to give a profound characterization of the devices. This would require a more extensive investigation which, of course, had to include PL spectra from sample #1 which had to be recorded over the hole angular range from 0 ° to 90 °. Anyway, the few measurements at angles of 20 ° and 5 ° which are shown in Figs. 2, 5 and 9 give evicence that the better performance of sample #1 accounts mainly for its longer resonance wavelength. It is better tuned to the gain function than the too short resonance wavelength of sample #2.

Considerable high intensities of the PL-spectra in laser operation, which can be observed in in Figs. 7 to 9 can be clearly attributed to the barriers of the structure. They reveal a serious loss mechanism which has to be considered in the quest for highly efficient devices. The presented measurement technique can be used for an elaborated examination of spectra from samples which are designed for reduced PL emission. A reduction of the PL from the barriers could be realized by means of avoiding the appearance of high carrier densities. Also a reduction of the volume of the barriers might be helpful in this context. Both can rigorously be realized by direct pumping of the quantum wells.

References

[1] S.W. Corzine, R.S. Seels, J.W. Scott, R.-H. Yan, and L.A. Coldren, "Design of Fabry-Perot surface emitting lasers with a periodic gain structure," *IEEE J. Quantum Electron.*, vol. 25, pp. 1513–1534, 1989.

[2] M. Kuznetsov, F. Hakimi, R. Sprague, and A. Mooradian, "Design and characteristics of high-power (>0.5-W cw) diode-pumped vertical-external-cavity surface-emitting semiconductor lasers with circular TEM_{00} beams," *IEEE J. Select. Topics Quantum Electron.*, vol. 5, pp. 561–573, 1999.

[3] S. Calvez, J. Hastie, A.J. Kemp, N. Laurand, and M.D. Dawson, *Thermal Management, Structure Design, and Integration Considerations for VECSELs,* in O.G.

Ohotnikov (Editor), *Semiconductor Disk Lasers*, Physics and Technology, Wiley-VCH, Weinheim, 2010.

[4] S.-S. Beyertt, U. Brauch, F. Demaria, N. Dhidah, A. Giesen, T. Kübler, S. Lorch, F. Rinaldi, and P. Unger, "Efficient gallium-arsenide disk laser," *IEEE J. Quantum Electron.*, vol. 43, pp. 869–875, 2007.

[5] J.-Y. Kim, S. Cho, J. Lee, G.B. Kim, S.-J. Lim, J. Yoo, K.-S. Kim, S.-M. Lee, J. Shim, T. Kim, and Y. Park, "A measurement of modal gain profile and its effect on the lasing performance in vertical-external-cavity surface-emitting lasers," *IEEE Photon. Technol. Lett.*, vol. 18, pp. 2496–2498, 2006.

[6] F. Demaria, S. Lorch, S. Menzel, M. Riedl, F. Rinaldi, R. Rösch, and P. Unger, "Design of highly efficient high-power optically pumped semiconductor disk lasers," *IEEE J. Select. Topics Quantum Electron.*, vol. 15, pp. 973–977, 2009.

[7] A. Hein, F. Demaria, A. Kern, S. Menzel, F. Rinaldi, R. Rösch, and P. Unger, "Efficient 460-nm second-harmonic generation with optically pumped semiconductor disk lasers," *IEEE Photon. Technol. Lett.*, vol. 23, pp. 179–181, 2011.

[8] F. Demaria and A. Hein, "Intra-cavity second-harmonic generation of blue 460 nm watt-level emission from optically pumped semiconductor disk lasers," *Annual Report 2009*, pp. 3–10. Ulm University, Institute of Optoelectronics.

[9] K.-S. Kim, J. Yoo, G. Kim, S. Lee, S. Cho, J. Kim, T. Kim, and Y. Park, "Enhancement of pumping efficiency in a vertical-external-cavity surface-emitting laser," *IEEE Photon. Technol. Lett.*, vol. 19, pp. 1925–1927, 2007.

[10] A. Hein and F. Demaria, "Bragg Mirror Design for Optically Pumped Semiconductor Disk Lasers Emitting at 920 nm," *Annual Report 2010*, pp. 121–128. Ulm University, Institute of Optoelectronics.